Proceedings of the 6th World Congress on Momentum, Heat and Mass Transfer (MHMT'21)
Lisbon, Portugal – June 17 – 19, 2021
Paper No. ICMFHT 102
DOI: TBA

FLOW BOILING IN PLAIN AND POROUS COATED MICROCHANNELS

Vivian Y.S. Lee[1], Gary Henderson[2], Alex Reip[3], Tassos G. Karayiannis[1]
[1]Brunel University London
Kingston Lane, Uxbridge, Middlesex UK UB8 3PH
Vivian.Lee@brunel.ac.uk; Tassos.Karayiannis@brunel.ac.uk
[2]TMD Technologies Ltd.
Swallowfield Way, Hayes, Middlesex, UK UB3 1DQ
Gary.Henderson@tmd.co.uk
[3]Oxford nanoSystems Ltd.
Blacklands Way, Abingdon, Oxfordshire, UK OX14 1DY
Alex.reip@oxfordnanosystems.com

Abstract - Flow boiling heat transfer enhancement using porous coatings in microchannels has been experimentally investigated. Results of the coated microchannel heat sink were compared to baseline results in a plain, micro-milled copper microchannel heat sink at similar operating conditions, namely inlet pressure of 1 bar, mass flux of 200 kg/m^{2}s and inlet subcooling of 10 K at wall heat fluxes between 24.5 kW/m^2 to 160.7 kW/m^2. HFE-7200 was used as the working fluid. Flow visualisation results and SEM surface analyses are presented. The coated surface was densely populated with well-defined cavities between 0.6 µm to 3.3 µm wide, while shallow but larger cavities up to 6 µm were found on the plain copper channels. Bubble generation frequency in the coated channels is significantly higher than in the plain channels due to the presence of more favourable nucleation sites on the coated surface. Flow pattern evolution occurred similarly in both heat sinks, namely bubbly to slug, churn and annular flow with increasing heat flux. Microchannel flow boiling heat transfer is enhanced by up to 43.5 % at low heat fluxes where the nucleate boiling mechanism is dominant. Heat transfer enhancement diminishes with further increase in heat flux to 13.2 %, potentially due to nucleate boiling suppression with flow regime transition.

Keywords**:** surface enhancement, porous coating, heat transfer, flow boiling, microchannels

1. Introduction

Efficient thermal management of high-power density devices constitutes a bottleneck in electronics miniaturization, where heat fluxes could reach several MW/m^2, Karayiannis and Mahmoud [1]. Traditional cooling strategies are insufficient in dissipating concentrated heat loads on modern high-power chip dies. This tends to limit the peak power output of a device in fear of compromising the junction temperature limit, reliability and performance of the device. Flow boiling in high surface-area to volume ratio microchannel heat sinks is a promising technique to manage high heat fluxes encountered in modern electronic devices and has been extensively studied, as reviewed in [1]. Nonetheless, issues such as flow instability, high boiling incipience temperature, dryout and critical heat flux and general predictive correlations for heat transfer and pressure drop need to be considered for this technique for compact cooling of miniaturised power components.

Some of these issues relate to bubble nucleation dynamics and surface wettability in the channel, and as explained in pool boiling work, surface defects and imperfections are favourable sites for bubble nucleation due to vapour entrapment [2]. Shojaeian and Kosar [3] reported that surface modification techniques such as altering surface roughness using sandpaper treatment, fabrication of artificial cavities and surface coatings have been employed to produce surface topologies with nucleation sites that may help to lower boiling incipient superheat, augment heat transfer and improve the critical heat flux limit in two-phase microchannel systems. Bai et al. [4] used three types of porous coating of different size structures on microchannel samples and found improvement in two-phase heat transfer coefficient by ~ 80 % at boiling incipience, but dropped significantly with further increase in vapour quality. Silicon nanowires enhanced heat transfer coefficient by up to 56 % in the work of Morshed [5] without apparent deformation of the nanowires after repeated experiments, which has been found in previous studies where the surface morphology of coatings degraded after several test runs [6]. The enhancement in two-phase heat transfer was attributed to the presence of preferable nucleation conditions for bubbles on the surface.

Hsu [7] as early as 1962 proposed a model to predict the size range of active nucleation sites on a heated surface. The model predicts that for a given working fluid and wall superheat condition, only a limited size range of nucleation sites may be activated to initiate bubble nucleation, i.e. boiling incipience on a heated surface. Using this model, surface characteristics may be optimised to provide an even distribution of cavities within the appropriate size range on the heated substrate, which is a more controlled method of cavity population compared to surface roughness modification and less complex compared to fabricating artificial nucleation sites in narrow passages.

In this study, a porous nanocoating is applied to a copper microchannel heat sink with 44 channels, produced by CNC micro-milling. The coating was applied on all three heated walls of the channels. The flow boiling behaviour of dielectric fluid HFE-7200 in a conventional CNC-milled copper microchannel heat sink is compared against the nanocoated sample of a similar configuration under the same operating conditions. The nanoFLUX® coating is a proprietary coating provided by Oxford nanoSystems Ltd. consisting of a metallic dendritic nano- and microstructure allowing for optimisable porosity for bubble nucleation. The inlet pressure, mass flux and inlet subcooling were fixed at 1 bar, 200 kg/m^2 s and 10 K respectively. The range of wall heat fluxes studied is between 24.5 kW/m^2 to 160.7 kW/m^2.

2. Experimental Methodology

The experimental facility is shown in Fig. 1 and the test section details are depicted in Fig. 2. The main loop consists of a reservoir, a gear pump, Coriolis mass flowmeters, a pre-heater, the test section and a condenser, which is cooled with ambient air aided by two axial fans. The copper microchannel evaporator has forty-four channels (i.e. N = 44) of width, W_{ch} = 0.36 mm, height, H_{ch} = 0.7 mm and length, L_{ch} = 20 mm, milled with a wall thickness of 0.1 mm on a 20 x 20 mm square area on the top of the copper block (D_h = 475 µm). The fin thickness, W_f, is 0.1 mm. The coated copper microchannels have similar dimensional values, with a slightly smaller hydraulic diameter, i.e. D_h ~ 456 µm, as a result of the coating (coating thickness ~ 5 – 10 µm). Five thermocouples were embedded in the block along the centre of the channels and 1.6 mm from the bottom surface to help measure the local heat transfer coefficient at the dimensionless axial positions: z/L = 0.17, 0.34, 0.5, 0.67 and 0.83 respectively. The inlet/outlet temperature and heat sink pressure drop are measured at the fluid line in the top plate. Flow visualisation was conducted along the channel at the centre of the heat sink as illustrated in Fig. 2, at a resolution of 512 x 512 pixels and 5000 fps for a duration of 1.3 s. Camera locations 1, 2, 3 and 4 refer to specific positions along the channels, which are the channel inlet, first centre, second centre and channel outlet. Each photograph covers a distance of 4.4 mm.

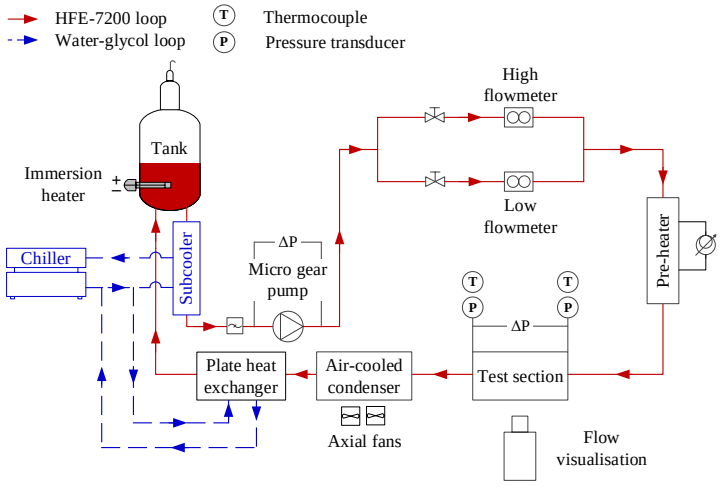

Fig. 1: Experimental flow loop.

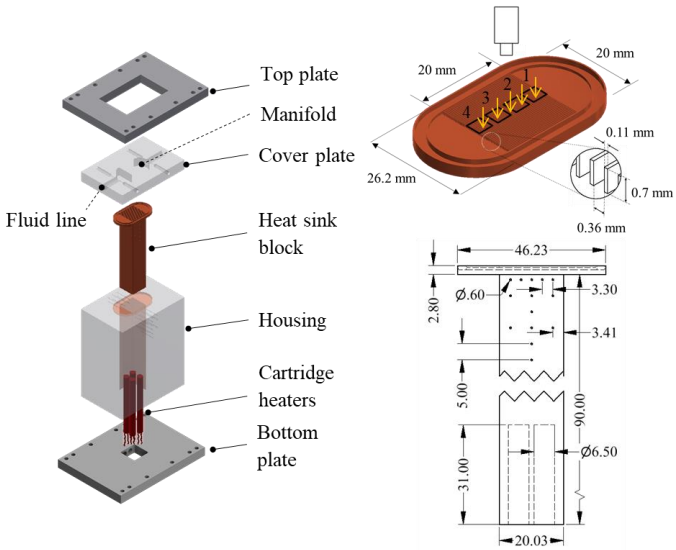

Fig. 2: Test section details.

The local heat transfer coefficient, $h_{(z)}$, is calculated as in Eq. (1), where $T_{f(z)}$ is the local fluid temperature, evaluated based on energy balance if in single-phase flow. The subcooled length, L_{sub}, was obtained based on the iterative method detailed in [8]. In the flow boiling region, $T_{f(z)}$ is the saturation temperature evaluated at the local saturation pressure based on a linear pressure drop assumption. The base heat flux q''_b was calculated using temperatures recorded by six thermocouples in the vertical direction. $T_{w(z)}$ is extrapolated from the axial thermocouple readings assuming 1D conduction. W_f, W_{ch}, H_{ch} and η are the number of channels, heat sink width, channel width, channel height and fin efficiency respectively. The fin efficiency is calculated assuming an adiabatic tip [9]. Further details of the data reduction procedure, including steps used to obtain single-phase friction factor, Nusselt number, channel pressure drop and details of the test facility can be found in [8].

$$h_{(z)} = \frac{q''_b \left(W_{ch} + W_f \right)}{\left(T_{w(z)} - T_{f(z)} \right)\left(W_{ch} + 2\eta H_{ch} \right)} \tag{1}$$

The average two-phase heat transfer coefficient, $\bar{h}_{tp}$, is obtained over the saturated length of the channel, which may be estimated by $L_{sat} = L_{ch} - L_{sub}$. The procedure to calculate L_{sub} is given in [8].

$$\bar{h}_{tp} = \frac{1}{L_{sat}} \int_{L_{sub}}^{L_{ch}} h_{(z)} \, dz \tag{2}$$

The percentage of heat transfer enhancement, E_{ht}, is calculated using the following equation:

$$E_{ht\%} = \frac{\bar{h}_{tp,coated} - \bar{h}_{tp,plain}}{\bar{h}_{tp,plain}} \times 100 \, \% \tag{3}$$

Data was acquired at a frequency of 1 kHz and for a period of 90s when all readings are in quasi steady-state conditions and do not vary in trend. Quasi steady-state is defined when the fluctuations are within ±0.2 g/s for mass flow rate, ±0.5 K for inlet/outlet temperature and ±0.05 bar for the inlet/outlet pressure over a period of at least 180 s. Live flow visualisation were also used to assess steady flow before data acquisition. Scanning Electron Microscope analysis was conducted on the LEO 1455VP at the Experimental Techniques Centre in Brunel University London. The propagated experimental uncertainties were evaluated based on the method described in Coleman and Steele [10]. The maximum uncertainty values of single-phase friction factor, single-phase Nusselt number, wall heat flux, two-phase heat transfer coefficient and vapour quality for the current experimental range are ±2.5 %, ±12.8 %, ±9 %, ±10.4 % and ±10 % respectively. Single-phase validation was conducted to verify the measuring instruments and data reduction method applied. Furthermore, the reproducibility of the experimental data was assessed and discussed in detail in [8]. For the results presented in the current study, the reproducibility of the heat transfer coefficient in the plain and coated channels exhibited a maximum mean absolute value of ±2.9 % and ±2.7 % respectively.

3. Surface Analysis

As reviewed in Mahmoud and Karayiannis [2], surface characteristics, fluid properties and operating parameters such as system pressure significantly influence the bubble nucleation process on boiling surfaces. Two-phase flow pattern development and flow boiling behaviour in microchannel systems are inevitably dependent on bubble nucleation, generation frequency and bubble dynamics. Since the working fluid and operating conditions were kept constant in both test sections, the primary difference in bubble generation frequency is likely to be caused by the difference in surface structure of the two test sections. To achieve a better understanding of the physics behind the effects of nanocoating on flow boiling results compared to the baseline plain microchannel results, the surface topography of the CNC micro-milled plain copper microchannels and the nanocoated microchannels were analysed using SEM.

Fig. 3 and Fig. 4 depict the surface characteristics of the channel bottom wall at a magnification of 5000x as measured on the plain and coated channels respectively. Examples of potential bubble nucleation sites are marked on each image. Surface defects produced by feed marks, smeared material and metal debris during the micro-milling process result in cavities that could potentially support bubble nucleation with sufficient surface superheat. On the contrary, a uniform layer of dendrite structures deposited in random orientations produce irregular pores that can potentially serve as nucleation sites on the coated surface. Cavities identified from the surface of the plain microchannel appear to be shallower, while cavities found on the

coated surface are more defined and seem deeper in comparison. Generally, the plain microchannel surface was covered with cavities of widths between 6 – 10 µm. However a few small cavities, ~ 0.7 µm in size, have also been identified. On the other hand, the treated surface was much more densely populated with small and medium size cavities with widths ranging from 0.6 to 3.3 µm. It is important to note that features in larger sizes suitable as nucleation sites on both the plain and coated microchannels may be found at lower magnifications on the SEM. The images shown in Fig. 3 and Fig. 4 are only a comparison between the two surfaces at the equivalent magnification. It can be concluded that there is an abundance of potential nucleation sites in the coated microchannels compared to the plain, CNC-milled microchannels. In addition, the cavities in the coated test section are more defined compared to the surface defects on the plain microchannels.

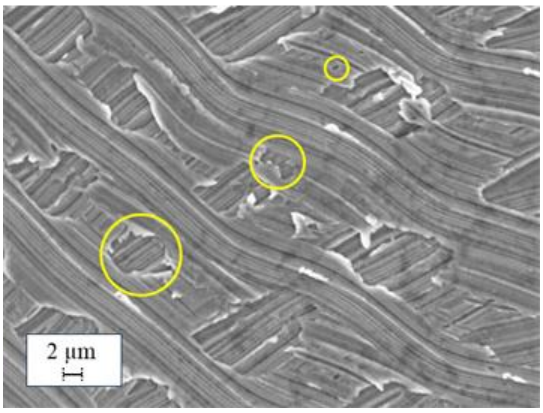

Fig. 3: Surface structure of the plain channel.

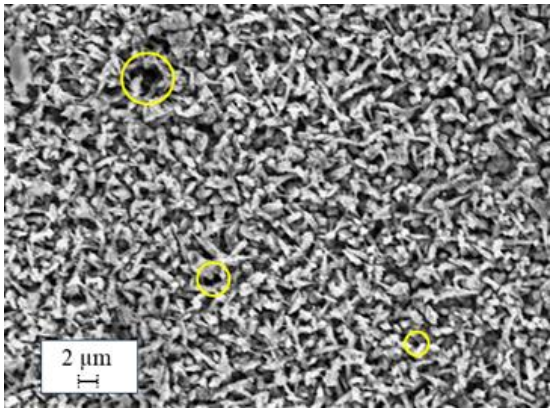

Fig. 4: Surface structure of the coated channel.

4. Results and Discussions

4.1. Single-phase validation

Single-phase adiabatic and heat transfer experiments were conducted in both test sections to validate the instruments used in the test facility The friction factor is plotted against Reynolds number in Fig. 5 and the experimental Nusselt number is shown as a function of Reynolds number in Fig. 6. For the adiabatic tests, the mass flux was varied from G = 250 – 2250 kg/m^2 s at inlet pressure and temperature of P = 1 bar and T = 40 ºC, while for diabatic tests, a base heat flux of $q_b^{"}$ ~ 5 kW/m^2 was applied across the same range of mass fluxes under similar operation conditions. .

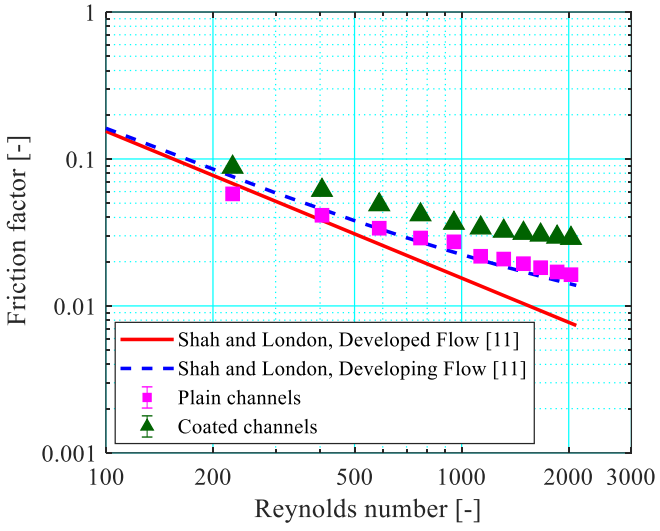

Fig. 5: Friction factor vs. Reynolds number.

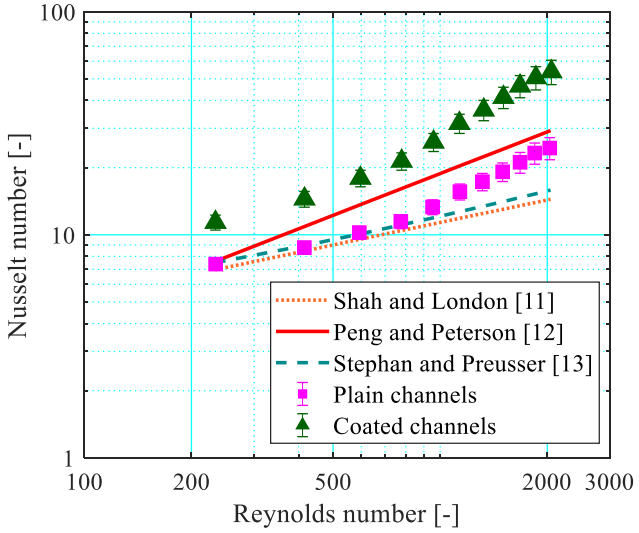

Fig. 6: Nusselt number vs. Reynolds number.

As mentioned above, the hydraulic diameter considered for the plain and coated channels are 475 µm and 455 µm respectively. The experimental results appear to be in good agreement with established prediction correlations summarized in Shah and London [11], Peng and Peterson [12] and Stephan and Preusser [13]. The friction factor and Nusselt number in the coated microchannel test section is higher than that of the plain test section. This may be attributed to the surface coating creating additional resistance to flow, increasing pressure drop in the channels. The higher experimental Nusselt number is a result of the enhanced single-phase heat transfer rates in the coated test section, which may have been promoted due to increased surface area and increased mixing by the coated surface.

4.2. Flow pattern evolution

Flow visualisation was conducted at four locations along the channel array to capture flow pattern evolution corresponding to each heat flux condition. High-speed recordings were conducted at 5000 fps and resolution of 512 x 512 pixels for a duration of 1.3 s at each location (see Fig. 2 for the locations). It is important to note that the high-speed recordings are not simultaneous. Flow visualisation was conducted when there are no significant changes in the measurements and flow pattern is observed to be quasi-steady. Hence the flow patterns captured, although not simultaneously at each location, remain a good representation of the flow pattern development along the channels. This was also verified by repeating the observations at two different occasions. Flow patterns observed in this study were categorised into bubbly, slug, churn and annular flow. The method of classification of flow regimes have been presented in [8]. As a result of the layer of coating on the top of the fins, there was some fluid transfer over the tops of fins as the top plate was not able to seal sufficiently. Nonetheless the flow pattern development in the channels was not significantly affected by this phenomenon and was mainly influenced by bubble ebullition and flow dynamics in the two-phase process. The layer of coating is ~ 5 – 10 µm in thickness. Therefore, the fins of the coated channels appear thicker compared to the plain channels. However, there is only a maximum of 4 % difference in hydraulic diameter between both test sections and thus remain comparable in the scope of this study. Photographs of flow regimes captured along the channel at the centre of the heat sink are shown in Fig. 7 at q_w" = 50.9 kW/m^2 and q_w" = 131.8 kW/m^2 for the plain channels and in Fig. 8 at q_w" = 50.4 kW/m^2 and q_w" = 125.2 kW/m^2 for the coated channels.

With increasing heat flux and vapour quality, two-phase flow pattern developed from bubbly to slug, churn and annular flow in the streamwise direction. Bubbly flow occurs at very low heat fluxes just after the onset of boiling in the channels. It is characterised by small bubbles nucleating from the side walls (Bubbly, Location 1, Fig. 7(a)) and isolated bubbles flowing within the bulk flow. Comparing the bubbly flow regime in the plain and coated channel, bubble nucleation is more active in the coated channels in this regime, as evident from the higher density of bubbles observed at Fig. 8(a) (Bubbly, Location 1) compared to in the plain channel.

Slug flow occurs when the isolated bubbles grow to the size of the width of the channels and become confined. With further growth in size, the bubbles elongate to form slugs in the channels, some of which may expand up to the full length of the channel. Intense bubble nucleation activity also promotes the establishment of slug flow due to increased bubble coalescence in the channels. Slugs have been observed to suppress active nucleation sites in the channels and also to migrate from neighbouring channels via the inlet plena through flow reversal, as noted in a previous study in [8]. However, the coated channels appeared to be less prone to nucleation site suppression as bubble nucleation activity and bubble generation frequency remained relatively high in the coated channels during slug suppression compared to the plain channels.

Churn flow occurs when the high velocity gas-phase within a slug forces the tip to collapse, breaking up individual slugs to form long slugs, with intermittent waves of a chaotic mixture of liquid and vapour accelerating toward the channel exit. Again, nucleation sites seem to be suppressed periodically in-phase with the intermittent and dispersed-phase churn wave. The churn regime captured in Fig. 7(b) (Churn, Location 2) and Fig. 8(a) (Churn, Location 3) show entrained vapour bubbles within the dispersed churn wave, which could have come from bubbles being stripped from their respective nucleation sites and entrained in the mixture as each wave accelerates downstream.

Annular flow develops after churn flow in the channels. Annular flow is characterised by a thin liquid film attached to the channel side walls with a vapour core in the middle of the channel. As mentioned above, long slugs have also been observed in the slug flow regime. The distinction between slug and annular flow respectively is the observation of isolated slugs in the interim between subsequent long slugs in slug flow and an uninterrupted vapour core in annular flow. Nucleation sites on the side walls remained active within the liquid film, as evident from Fig. 7(b) (Annular, Location 3) in the plain channel and Fig. 8(b) (Annular, Location 3) in the coated channel, but become suppressed with gradual thinning of the liquid film. Nucleation in the thin liquid film of annular flow was also reported by Borhani and Thome [14], Balasubramanian and

Kandlikar [15] and Al-Zaidi et al. [16]. As the layer is nearly depleted, the dispersed phase brought about by the intermittent churn flow rewets the channel walls and re-establishes a thin-liquid film on the channels. The annular liquid film in the coated channels exhibits a more irregular form.

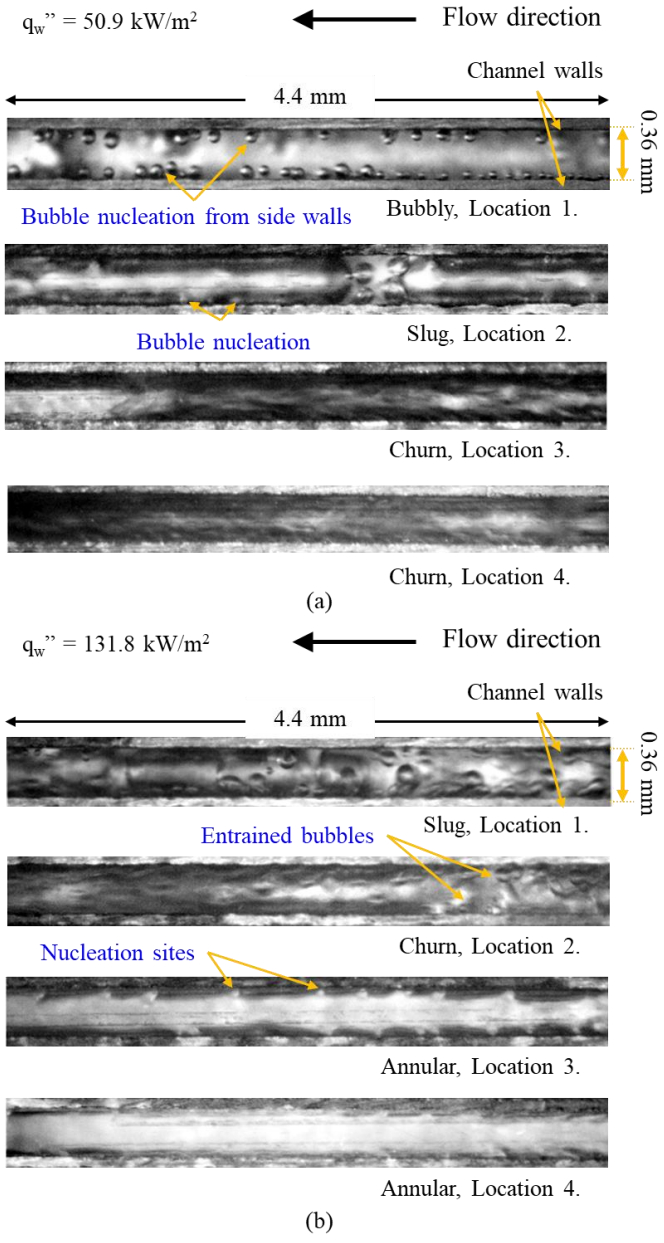

Fig. 7: Flow patterns in the plain microchannels at (a) q_w" = 50.9 kW/m² and (b) q_w" = 131.8 kW/m² (Locations depicted in Fig. 2.

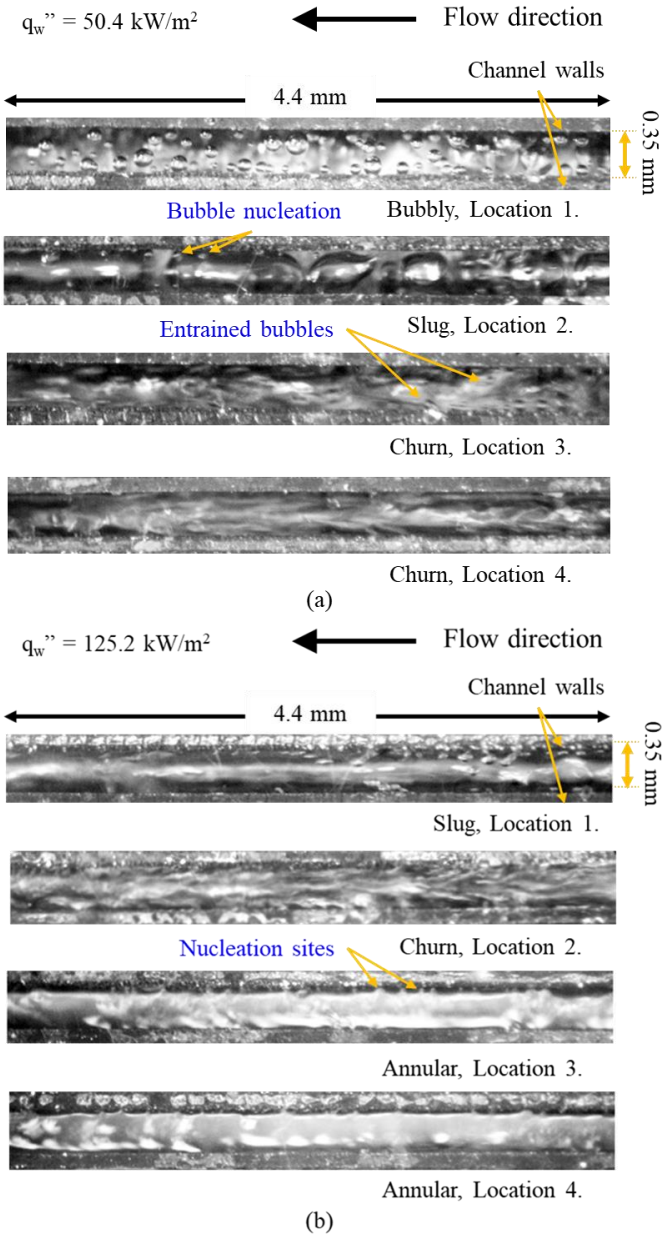

Fig. 8: Flow patterns in the coated microchannels at (a) q_w" = 50.4 kW/m² and (b) q_w" = 125.2 kW/m² (Locations depicted in Fig. 2).

4.3. Local heat transfer trend

Experiments were conducted in both test sections at a similar range of wall heat fluxes, namely q_w" = 26.1 – 160.7 kW/m² in the plain microchannel test section and q_w" = 24.5 – 153.3 kW/m² in the coated microchannel test section to investigate the effect of the nanocoating on microchannel flow boiling heat transfer performance. The applied heat flux was increased

gradually to result in an exit vapour quality range of 0 to 1. The experimental variables, including mass flux, inlet subcooling and inlet pressure were kept constant at $G = 200$ kg/m^{2}s, $\Delta T_{sub} = 10$ K and $P = 1$ bar respectively. As detailed above, local heat transfer coefficients are measured at five axial locations along the middle of the microchannel array in both test sections. Fig. 9 and Fig. 10 present the measured local heat transfer coefficients along the length of the channel as a function of local vapour quality in the plain and coated microchannels respectively. The respective vapour qualities at which flow pattern transition occurs, indicating flow pattern evolution as described in the section above, are annotated on the figures.

Generally, there is a peak in local heat transfer coefficient just after the onset of boiling in the plain microchannels. The initial peak is followed by a decrease in local heat transfer coefficient with increasing vapour quality along the channel. Near the channel exit, there is a modest increase in heat transfer coefficient. Similarly, a peak in the local heat transfer trend is seen in the coated microchannels near the start of the saturated boiling region. Local heat transfer coefficient followed a slight decreasing trend along the channel thereafter. The local heat transfer trends in the plain channels have been reported in detail in [8]. Contrary to the observations made in the plain microchannel, the local heat transfer trend near the channel exit does not appear to increase in the coated microchannel test section.

The steep rise in heat transfer coefficient at low heat fluxes ($q_w^{"} = 26.1 – 50.9$ kW/m^2), particularly in the subcooled region, is due to the change in main heat transfer mode from single-phase liquid convection to the more efficient nucleate boiling mode in the low vapour quality region where bubbly flow is observed. Subcooled boiling was observed in this study for both test sections. The peak is observed at low vapour qualities just after the onset of boiling, in the region where bubble nucleation activity is very high, and thus the nucleate boiling mechanism can be reasonably assumed to dominate. The high heat transfer coefficients could thus be due to the high heat transfer rates arising from micro-layer evaporation underneath a growing bubble and the mixing effects induced in the bulk fluid as a bubble departs its nucleation site [1]. A similar trend in the early stages of saturated flow boiling ($q_w^{"} = 24.5 – 50.4$ kW/m^2) is also observed in the coated microchannels.

The subsequent decline in local heat transfer trend with respect to vapour quality observed in both test sections could be due to suppression of the high heat transfer rates associated with the nucleate boiling mechanism following flow pattern development into slug, churn and annular flow. This is supported by the flow visualisation results presented above, where it is noted that bubble nucleation activity in previously active sites were observed to be suppressed, possibly due to flooding of the cavities, especially in intermittent churn waves and periodic liquid film dryout in slug and annular flow. Additionally, the transient variation of local heat transfer coefficient at a fixed location in the channels following transition slug flow could also have contributed to a drop in the time-averaged local heat transfer coefficient after the initial peak in heat transfer coefficient near the onset of boiling. Thome et al.'s three-zone model [17] predicts local heat transfer coefficients taking into consideration the periodic variation of heat transfer rates caused by (i) gradual thinning of the liquid film in slugs with film evaporation, (ii) local dryout following complete evaporation of the liquid film and (iii) the reinstatement of a liquid slug, which restarts the cycle of liquid film thinning, dryout and rewetting in the channels. Periodic dryout in the slug, churn and annular flow regimes were also observed in our flow visualisations and typically last ~ 100 ms. Although film evaporation rates increase with the thinning of the liquid film, relatively poor heat transfer coefficients are associated with the convective heat transfer occurring during the liquid slug stage and particularly in the dryout phase of the cycle. As a result, the time-averaged heat transfer coefficient at a particular location degrades after the onset of boiling and slug flow develops due to bubble confinement and coagulation in the channels.

The subsequent increase in the heat transfer coefficient near the channel exit of the plain microchannel test section could be due to (i) thinning of the liquid layer and (ii) conjugate effects in the heat sink occurring at the boundaries between the microchannel array and the inlet and outlet plena, as explained in [8]. The less pronounced effect observed in Fig. 10 could be due to the augmented heat transfer coefficients obtained from the coated test section in comparison with the plain test section.

Comparing the flow pattern transition lines in Fig. 9 and Fig. 10, it is clear that the bubbly flow regime persisted over a larger fraction of the plain channels compared to the coated channels. Bubbly flow transition into slug flow occurred earlier, at $x = 0.01$ in the coated channels compared to $x = 0.04$ in the plain channels. This could be due to higher bubble nucleation activity in the coated channels, as noted in the flow visualisation. On the other hand, slug-churn ($x = 0.068$ in plain channel

and x = 0.067 in coated channel) and churn-annular transition churn (x = 0.3 in both test sections) occurred at similar vapour qualities in both test sections. As mentioned above, slug-churn transition was observed to be induced by the collapse of slugs with increase with heat flux, while transition to annular flow occurs when a liquid film is deposited on the channel walls during intermittent churn waves. Individual slugs are broken up more easily when the velocity of the gaseous phase is higher, triggering flow pattern transition to churn flow. Similarly, a higher gaseous phase velocity promotes the establishment of a vapour core characteristic of annular flow. Superficial gas velocity, given by the ratio of mass flux (G) and vapour quality (x) over gas density (ρ_g), i.e. Gx/ρ_g [18] and widely used as a flow pattern transition criterion for slug-churn as well as churn-annular boundaries [19], can thus be reasonably assumed as a controlling parameter in transition to churn and annular flow. As the mass flux, inlet pressure and inlet subcooling, which affect flow parameters such as vapour quality and density are similar in both experiments, the superficial gas velocities do not differ significantly in the plain and coated channels. Unlike bubbly-slug transition, which occurred earlier in the coated channels, slug-churn and churn-annular flow transition boundaries occurred at almost identical vapour qualities in the plain and coated test section. This could be due to the similar superficial gas velocities for a given heat flux as well as mass flux and indicates that, for this geometry and ranged studied, transition to churn and annular flow is less influenced by bubble generation frequency, which as noted above, is significantly higher in the coated channels.

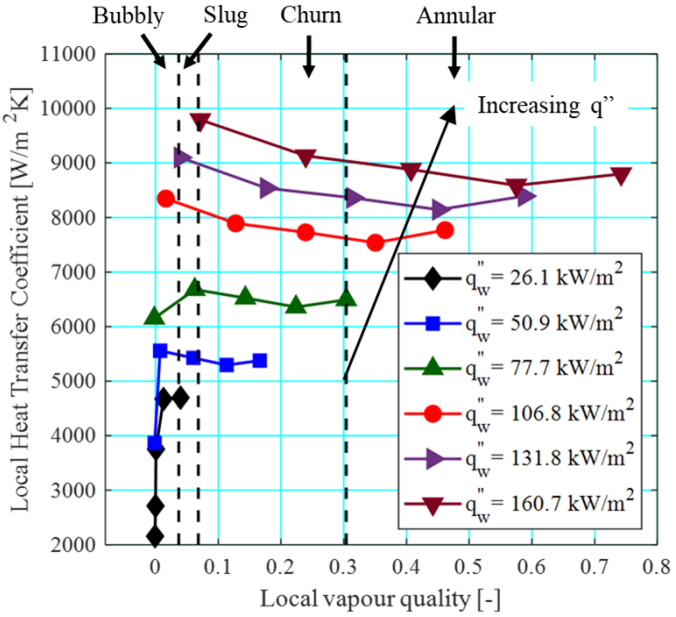

Fig. 9: Local heat transfer coefficient in the plain microchannels.

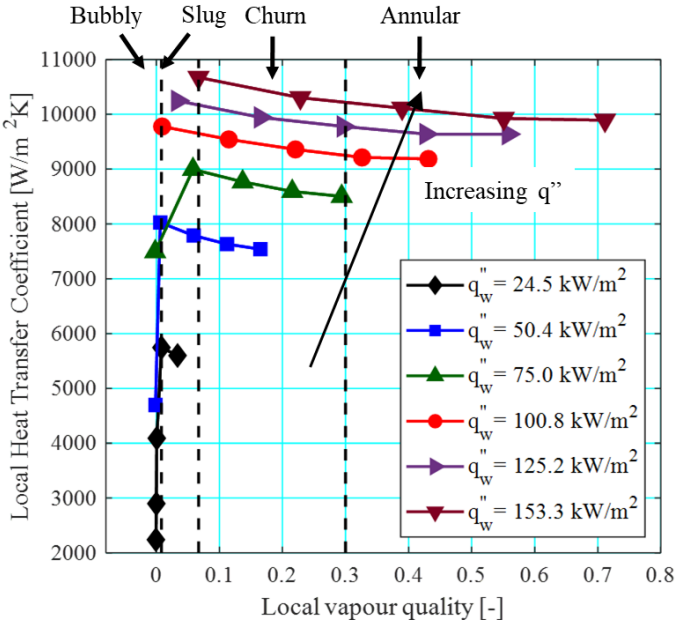

Fig. 10: Local heat transfer coefficient in the coated microchannels.

4.4. Average heat transfer coefficient

Overall, a clear increase in heat transfer coefficient with increase in wall heat flux can already be inferred from Fig. 9 and Fig. 10. To clarify the effect of wall heat flux on heat transfer coefficient in the plain and coated test section, the corresponding increase in average heat transfer coefficient (HTC) with respect to wall heat flux is plotted in Fig. 11. Two-phase heat transfer coefficient exhibits an ascending trend with increase in heat flux. Increasing wall heat flux increases wall superheat at the surface of the channels, which means that more potential nucleation sites may become activated. The correspondingly more vigorous bubble nucleation activity increases the average HTC value due to micro-layer evaporation and mixing currents induced by quenching at the wake of departing bubbles. Other than that, convective liquid film evaporation rate, which occurs around the perimeter of slugs and liquid films attached to the channel walls in churn and annular flow, may also increase with heat flux, see Thome and Consolini [20].

Importantly, the average HTC of the coated microchannel test section is superior to the heat transfer performance in the plain microchannels. Wall superheat was reduced by up to 3 K in the coated section for the current experimental range. The percentage of heat transfer enhancement relative to the plain microchannels (see Eq. (3)) is plotted in Fig. 12. There is an appreciable enhancement in heat transfer at the lowest heat flux level just after the onset of boiling, at 21.1 %, peaking at 43.5 % at q_w" ~ 51 kW/m^2. With further increase in heat flux and vapour quality (x > 0.22), there is a sharp drop in the heat transfer enhancement from 34.4 % at q_w" ~ 76 kW/m^2 to 13.2 % at the highest heat flux condition. A similar enhancement trend, that is, strong enhancement at the onset of boiling and depreciating enhancement with increase in vapour quality was also reported in Bai et al. [4]. As discussed in Section 4.2, bubble nucleation activity is higher in the coated channels compared to the plain microchannels at a given heat flux. This has been attributed to the abundance of potential nucleation sites in the coated channels compared to the plain channels due to cavities formed by dendritic structures of the coating on the surface of the coated channels. Where the main heat transfer mechanism is highly controlled by bubble nucleation, i.e. at and near the onset of boiling, where nucleate boiling is dominant, heat transfer enhancement should be relatively high due to the higher bubble nucleation activity in the coated channels. The moderate HTC enhancement of 21.1 % at the lowest heat flux (q_w" ~ 25 kW/m^2), where bubbly flow was mainly observed and wall superheat was just above 4 K, could be due to the activation of few nucleation sites in both test sections at such a low superheat condition. The range of active nucleation sites increases with increasing wall superheat, based on Hsu's model [7].

As the wall heat flux is increased to q_w" ~ 51 kW/m^2, wall superheat increases to around 7 K and a peak of 43.5 % in heat transfer enhancement is recorded. At this heat flux, bubbly and slug flow were observed upstream while churn flow developed downstream in both test sections. Notably, the bubbly flow regime occurred only very near the channel inlet of the coated test section, whereas bubbly flow persisted over a larger portion of the channels in the plain test section. It is clear from Fig. 4 that the cavities in the coated section are more defined compared to the surface defects seen on the bottom wall of the plain microchannels. Defined cavities may produce a stronger pinning effect on departing bubbles. This strong pinning effect may provide residual vapour pockets in the cavities from the preceding departing bubble, leaving behind a vapour embryo from which the subsequent bubble is able to grow from. This reduces the waiting time between subsequent bubble ebullition cycles, which could explain the higher bubble generation frequency in the coated channels and have been observed in our flow visualization, where higher bubble density in the channels were captured in the bubbly regime as shown in Fig. 8(a). Shallow surface cavities found on the plain microchannels may be less supportive for vapour entrapment, which increases waiting time (thus lowering bubble departure frequency) between subsequent bubble ebullition cycles in the plain microchannel test section. This is in addition to having a smaller number of cavities. As a direct consequence of higher bubble generation frequency and increased coalescence activity due to high bubble density in the coated microchannels, transition from bubbly to slug flow occurs at a much lower vapour quality in the coated test section than in the plain microchannel test section. Another possible enhancement effect could have resulted from the higher rate of heat transfer in the contact line between liquid slugs and the surfaces of the coated channels. Liquid film evaporation rate in the coated microchannels might have been promoted by increased wall turbulence with surface perturbations on the coated walls, as postulated as the reason for single-phase heat transfer enhancement.

Beyond q_w" ~ 51 kW/m^2, heat transfer enhancement degraded significantly with increase in wall heat flux. Churn and annular flow dominate the flow pattern in the channels at moderate and high heat fluxes. As shown in the flow visualisation results, bubble nucleation activity appears to be suppressed intermittently in churn flow while nucleation sites in the liquid film of annular flow are also periodically suppressed with gradual thinning of the film. As a consequence, heat transfer augmentation, which appear to be stronger when bubble nucleation activity is relatively high, drops in the region where churn and annular flow become dominant. The stronger mixing currents within the liquid layer on the rough coated surface continue to support some amount of heat transfer augmentation, albeit weaker than the enhancement obtained in the bubbly flow region where nucleation activity, or nucleate boiling, is the main contributor to heat transfer in the channels.

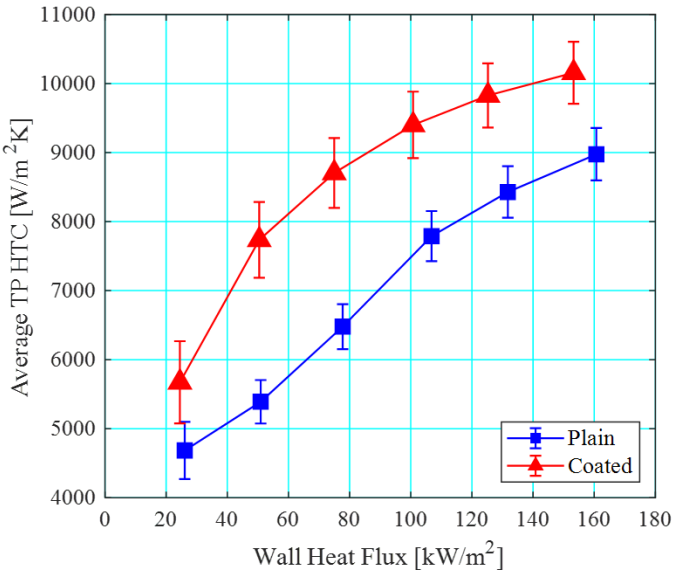

Fig. 11: Average two-phase heat transfer coefficient vs. wall heat flux in the plain and coated channels.

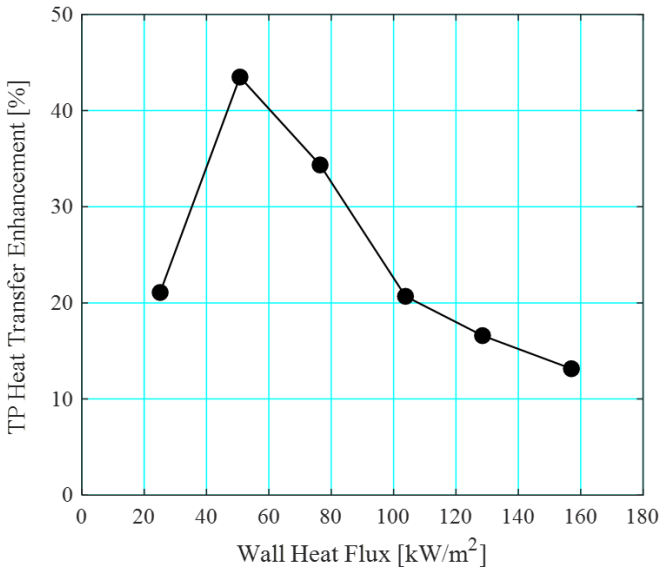

Fig. 12: Percentage of average two-phase heat transfer enhancement using the coated channels.

Conclusions

Experimental flow boiling results using HFE-7200 in a plain and coated copper microchannel heat sink were presented and compared at an operating condition of P = 1 bar at the inlet, G = 200 kg/m^{2}s, fixed inlet subcooling of 10 K for heat fluxes ranging from $q_w^{"}$ = 24.5 to 160.7 kW/m^2. The corresponding heat flux based on the footprint area of the microchannel heat sink (20 mm x 20 mm) was 93.7 – 614.9 kW/m^2. Flow patterns observed in this study were bubbly, slug, churn and annular flow. Similar flow pattern trends were observed in both test sections, with an earlier transition from bubbly to slug flow in the coated microchannels. This is due to higher bubble generation frequency in the test section, which was confirmed by flow visualisation. Higher bubble generation frequency in the coated microchannels is believed to be due to the higher density of potential nucleation sites available in the coated channels compared to the plain channels, as revealed by SEM surface analysis. Furthermore, the deeper cavities on the coated surface is believed to encourage vapour trapping, which results in lower waiting times between bubble ebullition cycles and thus increase bubble generation frequency. Subsequent slug-churn and churn-annular transitions were less dependent on bubble generation frequency and occurred at similar vapour qualities in both test sections.

Generally, local heat transfer coefficients peaked near the onset of flow boiling and decreased toward the channel exit. The peak in heat transfer coefficient just after the onset of boiling, where bubble nucleation activity is vigorous, is associated with high heat transfer rates in the nucleate boiling regime. The subsequent decrease in heat transfer coefficient may be attributed to increased nucleation site suppression and transient variations in heat transfer rate caused by dryout and rewetting cycles in the slug, churn and annular flow regimes. Average heat transfer coefficients increased with increase in heat flux, since more nucleation sites are activated in the channels with increasing wall superheat and liquid film evaporation rates become higher with increasing heat flux. Heat transfer enhancement was achieved using the nanocoated microchannel heat sink, in the range investigated in this study. The enhancement peaked at 43.5 % at $q_w^{"}$ = 51.0 kW/m^2 and dropped to 13.2 % at the maximum heat flux studied. The enhancement effect was found to be stronger at heat flux levels where nucleate boiling has a large contribution to the overall heat transfer, owing to the significantly higher bubble nucleation activity in the coated channels. The convective boiling mechanism could also have been enhanced by increased wall turbulence brought about by the coating structure on the channel walls.

Surface nanocoating has been shown to be a promising technique to enhance flow boiling heat transfer rates in microchannels, especially if the flow boiling system is operating at nucleate boiling dominant regimes. Preliminary assessment of the pressure drop data in the plain and coated heat sinks have shown that pressure drop across the heat sink was 5.9 kPa and 7.8 kPa respectively, at the highest heat flux in this study (~ $q_w^{"}$ = 160 kW/m^2). The relatively small pressure

drop values (due to the short channel length) demonstrated that the coating is a good method to enhance heat transfer rates in microchannels.

Acknowledgements

The authors would like to thank TMD Technologies Ltd. for their financial support and Oxford nanoSystems Ltd. for providing the coating for this study. The technical support of Costas Xanthos is gratefully acknowledged.

References

[1] T. G. Karayiannis and M. M. Mahmoud, "Flow boiling in microchannels: Fundamentals and applications," *Appl. Therm. Eng.*, vol. 115, pp. 1372–1397, 2017.

[2] M. M. Mahmoud and T. G. Karayiannis, "Flow Boiling in Mini to Microdiameter Channels," in *Encyclopedia of Two-Phase Heat Transfer and Flow IV*, J. R. Thome, Ed. World Scientific Publishing, 2018, pp. 233–301.

[3] M. Shojaeian and A. Koşar, "Pool boiling and flow boiling on micro- and nanostructured surfaces," *Experimental Thermal and Fluid Science*, vol. 63. Elsevier Inc., pp. 45–73, 2015.

[4] P. Bai, T. Tang, and B. Tang, "Enhanced flow boiling in parallel microchannels with metallic porous coating," *Appl. Therm. Eng.*, vol. 58, no. 1–2, pp. 291–297, 2013.

[5] A. K. M. M. Morshed, F. Yang, M. Yakut Ali, J. A. Khan, and C. Li, "Enhanced flow boiling in a microchannel with integration of nanowires," *Appl. Therm. Eng.*, vol. 32, pp. 68–75, 2012.

[6] C. S. Sujith Kumar, S. Suresh, L. Yang, Q. Yang, and S. Aravind, "Flow boiling heat transfer enhancement using carbon nanotube coatings," *Appl. Therm. Eng.*, vol. 65, no. 1–2, pp. 166–175, 2014.

[7] Y. Y. Hsu, "On the size range of active nucleation cavities on a heating surface," *J. Heat Transfer*, vol. 84, no. 3, pp. 207–213, 1962.

[8] V. Y. S. Lee and T. G. Karayiannis, "Effect of inlet subcooling on flow boiling in microchannels," *Appl. Therm. Eng.*, vol. 181, p. 115966, 2020.

[9] F. P. Incropera, T. L. Bergman, D. P. DeWitt, and A. S. Lavine, *Fundamentals of Heat and Mass Transfer 7th Edition*. John Wiley & Sons, 2012.

[10] Hugh W., Coleman, W. Glenn, Steele, *Experimentation, Validation, and Uncertainty Analysis for Engineers, 3rd Edition*. John Wiley & Sons, 2009.

[11] R. K., Shah, A. L., London, *Laminar Flow Forced Convection in Ducts: A Source Book for Compact Heat Exchanger Analytical Data*, 1st ed. Academic Press, 1978.

[12] X. F. Peng and G. P. Peterson, "Convective heat transfer and flow friction for water flow in microchannel structures," *Int. J. Heat Mass Transf.*, vol. 39, no. 12, pp. 2599–2608, 1996.

[13] Stephan, K., Preusser, P., "Wärmeűbergang Und Maximale Wärmstromichte Beim Behältersieden Binärer Und Ternärer Flűssigkeitsgemische," *Chem. Ing. Tech.*, vol. 51, no. 37, 1979.

[14] N. Borhani and J. R. Thome, "Intermittent dewetting and dryout of annular flows," *Int. J. Multiph. Flow*, vol. 67, pp. 144–152, 2014.

[15] P. Balasubramanian and S. G. Kandlikar, "Experimental Study of Flow Patterns, Pressure Drop, and Flow Instabilities in Parallel Rectangular Minichannels," *Heat Transf. Eng.*, vol. 26, no. 3, pp. 20–27, 2005.

[16] A. H. Al-Zaidi, M. M. Mahmoud, and T. G. Karayiannis, "Flow boiling of HFE-7100 in microchannels: Experimental study and comparison with correlations," *Int. J. Heat Mass Transf.*, vol. 140, pp. 100–128, 2019.

[17] J. R. Thome, V. Dupont, and A. M. Jacobi, "Heat transfer model for evaporation in microchannels. Part I: Presentation of the model," *Int. J. Heat Mass Transf.*, 2004.

[18] John G. Collier; John R. Thome, *Convective Boiling and Condensation*, Third. Clarendon Press, 1996.

[19] M. M. Mahmoud and T. G. Karayiannis, "Flow pattern transition models and correlations for flow boiling in mini-tubes," *Exp. Therm. Fluid Sci.*, vol. 70, pp. 270–282, 2016.

[20] J. R. Thome and L. Consolini, "Mechanisms of boiling in micro-channels: Critical assessment," *Heat Transf. Eng.*, vol. 31, no. 4, pp. 288–297, 2010.